IEEE Access
Multidisciplinary | Rapid Review | Open Access Journal

Received July 30, 2020, accepted August 4, 2020, date of publication August 6, 2020, date of current version August 19, 2020.

Digital Object Identifier 10.1109/ACCESS.2020.3014863

Decision Support System for Classification Medullary Thyroid Cancer

JAMIL AHMED CHANDIO[1,2,3], GHULAM ALI MALLAH[1], AND NOOR AHMED SHAIKH[1]

[1]Department of Computer Science, Shah Abdul Latif University, Khairpur 66111, Pakistan
[2]Larkana Institute of Nuclear Medicine and Radiotherapy (LINAR), Larkana 77150, Pakistan
[3]Sukkur IBA University , Sukkur 65200, Pakistan

Corresponding author: Jamil Ahmed Chandio (jameelahmed.phdcs@iba-suk.edu.pk)

This work was supported by the Department of Computer Science, Shah Abdul Latif University, Khairpur, Pakistan.

ABSTRACT Due to the complex, heterogeneous and mimic morphological features of medullary thyroid cancer (MTC). It becomes often difficult to diagnose MTC at early stage. Since histopathological complex patterns of cancerous cells and tissues requires a huge effort to classify. Therefore thyroid cancer classification has become one of the significant research area area(s) of Machine Learning. We propose a decision support system to classify initial variation of morphological appearance of nuclei by using Convolutional Neural Networks (CNNs). The system comprises over three major layers, where image preprocessing techniques are used at top layer along with feature selection techniques. Classification model constructed by using CNNs at the second layer and result visualization described at third layer. Due to the unavailability of datasets for medullary thyroid cancer in literature, this research uses real-world datasets consisting upon 20GB cytological medical images and the approximated classification accuracy is measured about 99.00%. Malignant and non – malignant cells are visualized to assist the doctors in better way.

INDEX TERMS Histopathology, thyroid cancer, classification, machine learning.

I. INTRODUCTION

Although every cytological medical image contains useful information for malignant diseases but inference of each image in terms of machine learning requires systematic approach to explore the hindsight knowledge for diagnostic purposes. Histopathological image classification needs significant efforts to classify, because every cancer has dissimilar, mimic and complex features [1], [2]. Often noise reduction techniques need to be optimized carefully because relevant information may be lost by applying improper segmentation techniques as shown in [Figure 1] and [Figure 2]. There is verity of segmentation techniques [3], [4]. Such as graph cut, threshold, super pixel and other segmentations, but for every medical image; each technique could not produce fruitful results [5], [6]. Therefore medical image mining has become one of the recognized research area(s) of machine learning. Recently many CAD (Computer added diagnosis) systems were proposed to diagnose such as lung [7], [9], liver [10], [12], thyroid and others cancers by using medical images but minor variations in nuclei eccentric properties are need to be visualized to assist the doctors in more effective way [13], [16]. Since the nucleus deviation from its central point is an alarming variable to be considered for diagnosis of abnormalities among the tissues of MTC; because minor variation in the spatial location of nuclei could be over sighted which may become one of the leading cause of misdiagnosis. Therefore careful investigation of nuclei grooves may provide more validate results of the diagnostics. Thyroid hormones refreshes to every cell of human body and regulate functional status of human organs. Structural changes badly effects the functional status of the thyroid gland where it may release low or high amount of thyroid hormones. At the initial changes thyroid hormones assessment may be noticed with low or high production of hormone in thyroid papillary, follicular cancers whereas in medullary thyroid cancer the functional assessment is very difficult to examine. Most of times medullary thyroid cancer may palpable at advance stages and it may become very difficult to treat and cure it. In literature [26]–[32] some approaches are seen to classify the medical images of ultrasonic and cytological material where above stated optimization may enhance the quality of CAD systems. This article proposes a novel approach so called ''Decision Support System for Classification of Thyroid Medullary Cancer'', which offers a classification system to predict malignant behaviors of MTC

The associate editor coordinating the review of this manuscript and approving it for publication was Jeon Gwanggil.

and visualizes eccentric nuclear behaviors within cells of MTC. The system is divided into three layers at the first layer, image preprocessing where feature selection techniques are used and objects are detected in shape of nuclei; meanwhile coordinate, regional maxima based features are extracted for transformation of datasets, Such as Eccentric nuclei (EC) and chromatin energy levels (CEL). At the second layer classification model constructed to find out dependencies among the associated variables by using CNNs. Third layer is devoted to perform the result visualization where confusion matrix, precession and recall measures are used. Measured classification accuracy for this approach is recorded as 99.00%. On the same layer visualization of eccentric nucleus is shown. Due to the unavailability of such datasets real-world datasets we acquired the cytological images from SMBBMU (Shaheed Muhtarma Be-Nazeer Bhutto Medical University), Pakistan.

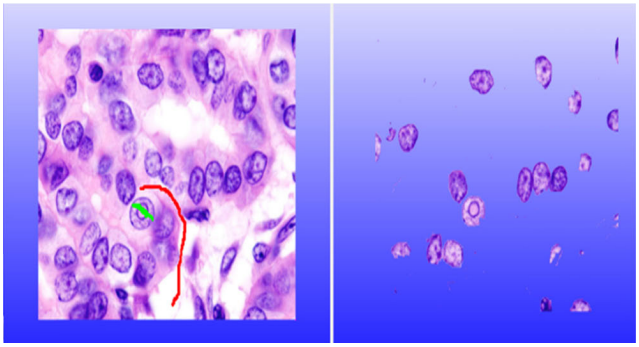

FIGURE 1. Graph cut segmentation on the similarity basis.

A. NOISE REDUCTION TECHNIQUES

Image preprocessing techniques are widely available in literature. Since cytological image noise reduction is a unique problem because each nuclei is to be detected carefully with its all micro- architectural components from cell wall to deepest component so called nucleus. Each component reveals information about the existence of cancer disease therefore must be included and minor variation may be recorded in training dataset because testing dataset may provide more better results if training dataset contains deepest information of the cytological material. Some of the noise reduction techniques are given bellow.

Graph cut segmentation [17]–[19] uses similarity index of RGB combination, let's consider $x\epsilon\{\text{RGB }\}\text{N}$, where S ϵ RN carries foreground and background information which is to be partitioned on the basis of cuts as shown in above [Figure 1]. P $(x\backslash\text{S})$ K- E where E assigns two function to detect the objects such colour and coherence.

Threshold segmentation [20]–[22] creates two partitions of the objects based upon the high and low pixel values ranges from 0 to 255 energy levels. The pixels. These images are also called grey scale images. Each pixel $I = i, j$ is loaded into the feature vector and performs object detection on the basis of T value where T is represented as threshold. Image partitions are performed if $I = i, j > T$ *or* $I = i, j < T$; meanwhile watershed transformation forms clusters of objects by considering the connected objects with boundaries. Canny edge detection performs basic operation to detect the boundaries of the objects and sub objects.

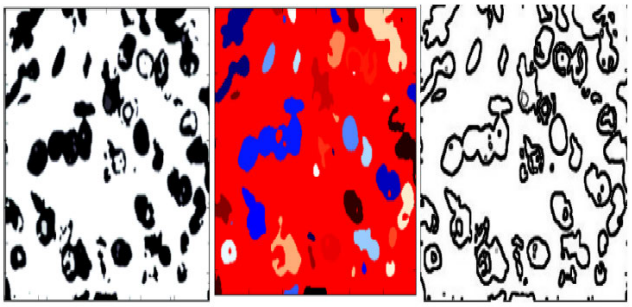

FIGURE 2. Threshold segmentation, Watershed segmentation, canny edge detection.

B. CONVOLUTIONAL NEURAL NETWORK

Convolutional neural networks (CNNs) falls into the class of deep learning. CNNs are applied in verity of application of visual fields consisting upon the filters also known as kernels. Small receptive field carries information of every pixel and it extends up to in-depth to fully connect by processing as input by convolve width and height of the volume. CNNs architecture comprises over convolutional layer, where sparse local connectivity uses neuron patterns of adjacent layers [23], [24], and [25]. In CNNs pooling layer performs operations over linear and nonlinear inputs. The layer is also called max pool because it is responsible to handle maximal limits of the data by summarization [26], [27]. The max pool layer performs input / output reduction operation by following the assigned parameters. The layer detects the objects by forming the rectangles. Rectified linear unit (ReLU) works on non-saturated activation functions where $f(x) = max(0, x)$. It forms hyperplane between the object in such a way that $(x) = tanh(x)$, $f(x) = |tanh(x)|$ becomes satisfied with sigmoid function exponentially. Fully connected layer tackles all outputs received from previous layers by using matrix multiplication [28]. By considering the accuracies received from the loss layer and drop out layer is used as weight to enhance the classification accuracy of visual objects.

II. LITERATURE REVIEW

Many CAD systems were proposed to diagnose thyroid cancer disease by using the ultrasonic and histo-pathological images of histopathological images so called FNAB (Fine Needle Aspiration Biopsy). Some of related works to predict the malignant cells and tissues are given below.

Thyroid follicular cytological images were classified by using multiple instance learning [29]. The whole cytological images were trained and local image features score were assigned to classifier to find out the similar cancer cells and tissues. Supervised learning method was used to extract the region of interest and classification results show that 87.00 % accuracy was obtained whereas we classify the medical

images of FNAB for classification of medullary thyroid cancer and obtained 99.00% classification accuracy.

Thyroid follicular, papillary, anaplast, medullary cancer classification was proposed [30], deep convolutional neural network was used to classify. Training images were annotated by filliping images at and segmentation of pathological images was performed by using Laplacian Gaussian filters. Classification accuracy for medullary thyroid cancer was 97.77% whereas we classify the nuclei eccentric property for medullary thyroid cancer by considering each individual nuclei and we obtained 99.00% classification accuracy for medullary thyroid cancer.

Papillary thyroid cancer classification technique was proposed [31] by using ultrasound images, deep learning algorithm was used to perform classification operation and reported accuracy was measured as 93.5%, whereas mostly doctors rely on histopathology technique. Therefore biopsy is considered as gold standard for cancer diagnosis. We use histopathological images and received 99.00% classification accuracy.

A comparative study [32] was conducted to classify the thyroid nodules by using ultrasound. The nodules were classified in five categories as proposed by [30] and the best accuracy was recorded 89% for class five; whereas we propose a system, which is fully automated and micro architectural level features such as analysis of nucleus is considered as key component to predict the malignant nodules existing in the bunch of nuclei on a FNAB (Fine Needle Aspiration Cytology).

A system [33] was proposed to compare the nodular enlargements by using FNA (Fine needle Aspiration) cytology and ultrasound features. Overall accuracy of the system was measured as 73%. This article proposes a system which not only extract the features for visualization of nucleus but also predicts eccentric nuclei patterns to confirm either the nuclei is suspicious for malignancy or not.

A system [34] was proposed for classification of leukemia disease to analyses the cell level features by using the FNA (Fine needle Aspiration) cytology. The overall classification accuracy shown as per author is 98.5%. As per our proposed technique, since the classification problem of lymphatic suspicious nodules needs significant effort to analyses the behaviors and properties at the micro-architectural levels.

A leukemia segmentation approach [35] was proposed for classification of leukemia disease. The proposed algorithm uses watershed segmentation to visualize the WBC cells of blood and their correlations, whereas we visualize deepest knowledge of medullary thyroid cancer with approximated 99.00% accuracy.

A method [36] for thyroid cancer diagnosis was proposed by using ultrasound images. Region of interest was selected from the well acquired ultrasonic echo of thyroid region and median fitters were applied to reduce the noise. Active counter based features was extracted for training and testing data. Multilayer perceptron and support vector machines were used to build the classification model. 94.44% accuracy was obtained, whereas we received 99.00% classification accuracy for MTC.

A computer added diagnostic system [37] for thyroid cancer classification by using ultrasound images was presented. A radiology expert selected regions and Gabor filter was applied to de noise the echo generated by the ultrasound image. 83.85% accuracy was obtained for diagnosis of papillary thyroid cancer. Doctors rely on histopathological findings because biopsy known as gold standard.

This article proposes a novel system from the three perspectives; such as (i) each nuclei has given equal chance to be classified (ii) eccentric nuclei properties are visualized (iii) highest classification accuracy 99.00% for MTC has been obtained.

III. METHODOLOGY

Methodology of proposed system falls into the predictive mining classification and it deals with the histo-pathological images to predict the malignant medullary thyroid cancer cells and tissues at initial stage.

Dataset: A real-world dataset was received from Shaheed Muhtrma Benazir Bhutto Medical University, Pakistan for the year 2018-2020. The dataset was comprising over 100 histopathological images of medullary thyroid cancer. Image acquisition was done by using high resolution microscope. Average size of each image was received with x100 magnification power and 4000 $\times$ 2500 pixel size per image. Due to high density of histopathological objects, image pre-processing operations were applied for efficient training and testing of machine learning techniques such convolutional neural network. There are serval number of micro architectural components such as Chromatin, cell wall, nucleus and others, we recorded the nucleus based features. Approximated 5601 nuclei were auto-cropped; consisting upon 20 x 20 pixels in average size. The size of converted grey level nuclei was measured as 28 x 28 pixels [Figure 7]. Colour movements for each nuclei were obtained as per [Figure 8], where nuclei shapes are shown and their locations are demonstrated with x and y location. Colour movements of RGB combination are visualized in columns by using features of grey level intensity, centroids, locations and class label attributes where each selected nuclei was carefully labelled as per decisions of doctors. Each colour of nuclei's estimated from the dimension of morphology, size, location and other features. We prepared two datasets; where first dataset contains set of nuclei with doctor defined class label attribute and second dataset contains information about the nuclei neighbors, centroids and their locations, which are visualized either belonging to the category of malignant or non-malignant.

A. LAYER 1: IMAGE PREPROCESSING

Histopathology images for medullary thyroid carcinoma contains micro architectures such as cell wall, chromatin distribution, nucleus and others. In this article we preprocess each nuclei in such a way that nuclei can be auto-cropped and human involvement may be reduced. We focus on nucleus

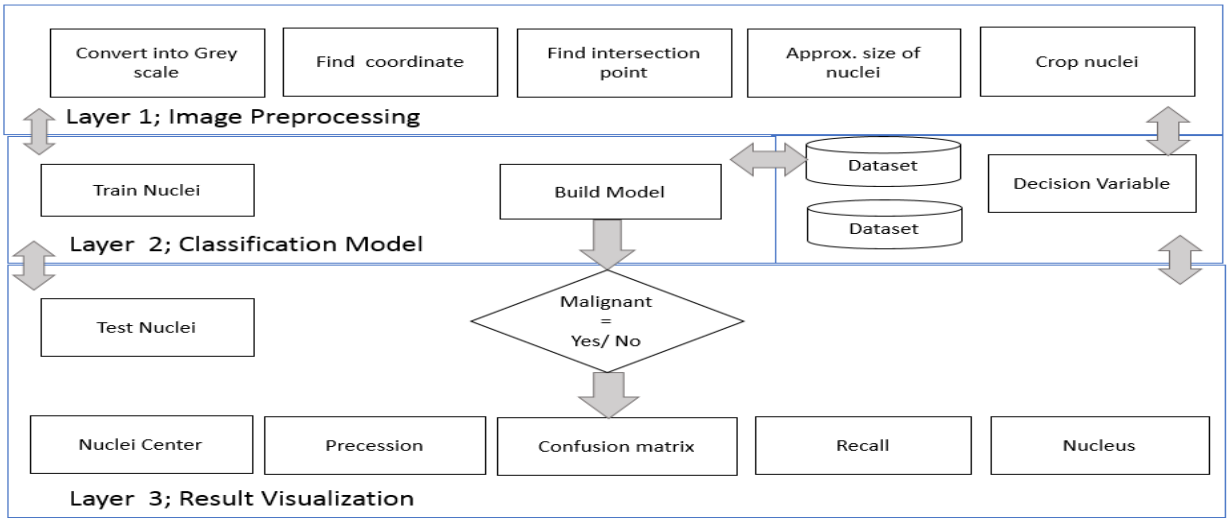

FIGURE 3. Decision support system for medullary thyroid Cancer Workflow.

eccentric features for diagnosis purpose. Let's consider each micro architecture is an object which may be located at any coordinate of the medical image considered as $object^1$, $object^2$, $\ldots\ldots\ldots object^n$ and set of objects are assumed as $Nuclei^1, Nuclei^2 \ldots\ldots\ldots Nuclei^n$. Every histopathological image may contain infinite number of nuclei but due to limitation of microscope image acquisition; a finite number of nuclei are visible over single histopathological image. There are two points for each nuclei where vertical could by supposed as initial point and horizontal ending point which may be represented by x and y locations. The intercept of both points would be assumed as nucleus of nuclei; meanwhile z variable carries information of intensities of pixel depth.

1) CONVERT INTO GREY SCALE

Grey scale image segmentation is considered as gold standard because intensity of each segmented pixel could easily quantified. Ostsu threshold segmentation technique was used to de-noise the histopathological images where each pixel intensity ranges from 0 to 255. A nuclei is supposed to be found with variation in circular shapes and morphometric behaviors. There are fair chances of malignancy having evidence of eccentric nucleus property. The appearance of nuclei with minor variation look like a normal nuclei in colour images but on careful observation show that pixel energy level provides more precise result to measure the abnormality of each nuclei. Let's consider proposed iteratively method of this article, a histopathological image is collection of MXN matrix where each nuclei is represented with pixels and every pixel is situated in x and y coordinates. Therefore a set of objects so called nuclei could be assigned for user defined threshold segmentation as defined in eq. (1) where $\frac{\partial f}{\partial x}, \frac{\partial f}{\partial y}$ carries information of each pixel intensity in the form of first derivative and created a feature vector.

$$\nabla f = [\frac{\partial f}{\partial x}, \frac{\partial f}{\partial y}] \tag{1}$$

A feature vector of first derivatives assigned several number of objects and grey pixels were identified with gradient function. Mean intensity gradient is used for segmentation as represented in eq. (2) Image partitions are performed if $I = i, j > T$ *or* $I = i, j < T$ as shown in [Figure 4].

$$\theta = tan^{-1}(\frac{\partial f}{\partial x} / \frac{\partial f}{\partial y}) \tag{2}$$

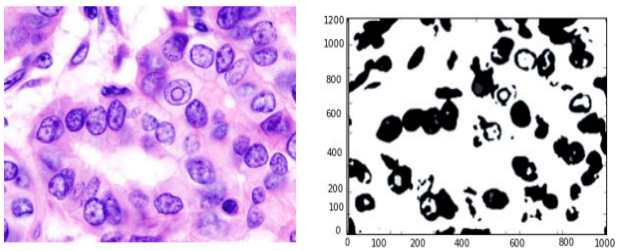

FIGURE 4. Conversion of colour to grey scale image.

However second derivation as binary segmentation has converted set of nuclei in foreground and background set of images eq. (3). $\sqrt{\left(\frac{\partial f}{\partial x}\right)^2 + \left(\frac{\partial f}{\partial y}\right)^2}$ Where $\frac{\partial y}{\partial x}$ carries foreground and $\left(\frac{\partial f}{\partial x}\right)^2$ back ground information of image but by considering threshold T, The clusters of nuclei converted into grey scale for further processing to find out the coordinates.

$$\| \nabla f \| = \sqrt{\left(\frac{\partial f}{\partial x}\right)^2 + \left(\frac{\partial f}{\partial y}\right)^2} \tag{3}$$

2) FIND COORDINATES

Let's consider that noise reduction have been done by eq. (3) and G = (x, y) position is equal to the centre of nuclei forming the edges to be represented as eq. (4) where $\frac{dy}{dx} = (x, y)$ is location where edges of the objects contains circular quantities in equal intervals $[x + 1]$ as nucleus of the set of nuclei

as shown in [Figure 5].

$$\frac{\partial f}{\partial x}[x, y] \approx f\,[x+1, y] - f[x, y] \tag{4}$$

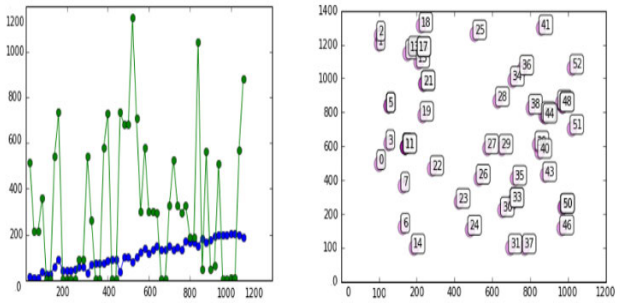

FIGURE 5. Finding coordinate of nuclei.

3) FIND INTERCEPT POINTS

Each circle is created by considering the center of most intensity releasing set of pixels where $\frac{dy}{dx}$h ∗ f has to develop a circle around the each nuclei and consider the same as eccentric nuclei eq (5).

$$\frac{\partial}{\partial x}(h*f) = \left(\frac{\partial}{\partial x}h\right) * f \tag{5}$$

By counting the area of nuclei as foreground during the segmentation process and colour intensities are recorded as per eq (6) where both image partitions $\frac{\partial^2 f}{\partial x^2} + \frac{\partial^2 f}{\partial y^2}$ are transformed by considering the centric and eccentric nuclei as shown in [Figure 7]. All above points were recoded into dataset by considering as distance matrix because distance matrix is the formal representation of set of objects where unique position for each object could be processed for auto-cropping of nuclei but the central point and set of connected pixels is the key to execute the function.

$$\nabla^2 f = \frac{\partial^2 f}{\partial x^2} + \frac{\partial^2 f}{\partial y^2} \tag{6}$$

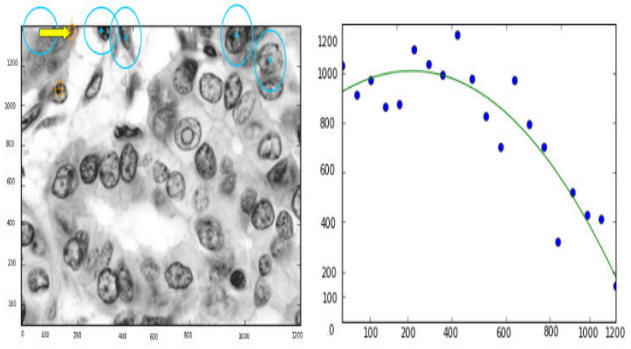

FIGURE 6. Intercept locations for nuclei.

4) APROX. SIZE OF NUCLEI

In cytological images, the size of cells is not fixed. Thus proper approximation of cells was done before cropping them. Since the height, width, diameter and their coordinated are required to not measure the size of nuclei but also on the basis of above parameters we may crop them. As the image was converted into grey scale therefore every object has three properties ($image = (x, y, z)$ locations which were excreted as $G = (x, y)$ where G is the unique centroid position of the object and x, y locations were depending up on intensity $I = (x, y)$ where all intensities of possible edges where recorded by considering z variable. On the basis of above variables a decision matrix was constructed where information of centroid and object neighbor was recorded to crop the nuclei.

5) CROP NUCLEI

Let's consider eq. (5) where $\left(\frac{\partial}{\partial x}h\right) * f$ finds the set of connected pixels and approximate the average central point for a processed object so call nuclei and eq. (6) where each image is transformed by emerging the second derivative function and recorded quantities for neighbor set of same intensity of pixels, calculated set of connected pixels is considered as are of each nuclei and involved area could be cropped by fitting the values for each nuclei [Figure 7] as calculated above.

FIGURE 7. A view of pre-processed dataset to be processed with CNNs.

6) CONSTRUCT DATASETS

Where each cell wall has to qualify the threshold as defined in eq. (7) where $g(x)$ is unique object location and the same is to be plotted into the colour matrix and histogram to measure the colour based feature by using RGB combinations [Figure 8].

$$\mathrm{g}\,(\mathrm{x}) = \begin{cases} \geq & 1 \\ < 0 & otherwise \end{cases} \tag{7}$$

After acquiring the grey scale set of nuclei we applied the Euclidian distance algorithm to extract the coordinates of nuclei and applied watershed algorithm to label the points of coordinates. Finally doctors included class label attribute for every image, in this way, we recorded more than 5601 observations for training and testing dataset.

B. LAYER 2: CLASSIFICATION MODEL

We trained classifier Convolution neural network (CNN) to perform classification operations. Although CNNs based

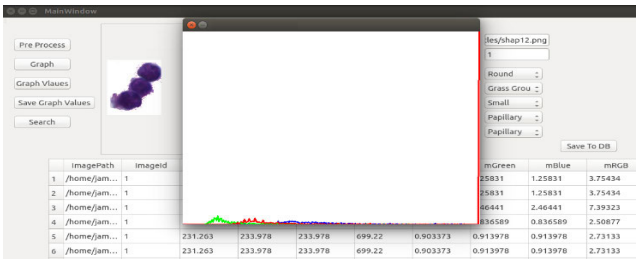

FIGURE 8. Feature extraction for plotting nuclei centre and nucleolus.

classifiers uses image filters at each layer but each nuclei should be provided equal opportunity to classified therefore we performed image pre-processing where each nuclei extracted from the very dense cytological images of medullary thyroid cancer. Huge size cytological image were consisting upon 4000 × 2500 pixels per image but we auto cropped nuclei with 28 x 28 pixel as per our proposed method defined at layer one. Weights as well as model architecture design enhances the performance of the classifier and doctors received additional assistance to predict malicious cells and tissues from the whole dataset individually.

TABLE 1. Architectural summery for CNN.

Layer Type	Kernel size	Feature Map
Input image	28 x 28	----
Convolutional Layer-1	3 x 3	28 , 28, 32
Drop out Layer- 1	5%	--
Zero Padding Layer-1	3 X 3	26,26,32
Max pooling -1	2 x 2	13,13,32
Convolutional Layer-2	3 X 3	26,26,64
Drop out Layer- 2	5%	--
Zero Padding Layer-2	2 x 2	26,26,64
Max pooling -2	2 X 2	11,11,64
Convolutional Layer-3	3 x 3	26,26,128
Drop out Layer- 3	5%	--
Zero Padding Layer-3	1 X 1	5,5,128
Max pooling -3	2 x 2	3,3,128
Fully connected Layers	32	-
Fully connected Layers	64	-
Fully connected Layers	128	-

We trained classifier over three convolutional layers such as 32, 64,128 and fitters with 3 x 3, 2 x 2, 1 x 1 were applied at stages whereas for max pooling layer 3 fully connected layers were designed at experimental setup to find out the deepest knowledge [Table 1]. Convolutional layer 1 was assigned 3 x 3 size of kernel function where 28, 28, 32 parameters were processed. The dropout 5 % was fixed for each layers. Padding was initialized with 26, 26, and 32 because when we received output of classifier at first compilation it gave 26 quantity. The max pooling for layer one as 13, 13, and 64. Second convolution layer assigned 26, 26, 64 parameters with same dropout and max pooling layer compiles 11, 11, 64 quantities. Layer number third was assigned 26, 26, 128 parameters. Drop out remained same and padding layer 5, 5, 128 parameters whereas max pooling parameters remained 3, 3,128.

In [figure 9] some of epochs for fully connected layers are presented.

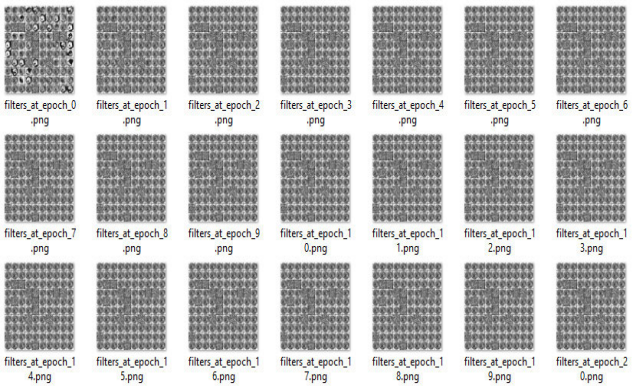

FIGURE 9. A view of epochs generated by classifier.

C. LAYER 3: RESULT VISUALIZATION

Accuracy of the proposed system is calculated by using confusion matrix, where classifier performance in terms of true and false positive values are acquired as per eq. (8). The confusion matrix is also called identity matrix where quantities of classified could be seen diagonally.

$$Accuracy = \frac{Sum\ of\ True + ve\ and\ False - ve}{Sum\ of\ All\ False, True + ve\ and - ve} \tag{8}$$

Precision is a measure which is collection of true positive vote counts divided upon the number of observations either belongs to true and false positive. The precision shows that how much observation are understood by the classifier eq (9).

$$Precision = \frac{Number\ of\ True\ Positives}{Number\ of\ True\ Positives + False\ Positives} \tag{9}$$

The recall measure consists upon the true positive observation divided by the false positive instances. The recall measure shows that what would be the probability for the testing observation eq. (10). Precision are those observations which are comprehended by the classifier whereas recall is the ability of the classifier to predict the unknown observation.

$$Recall = Sensitivity = \frac{True\ Positive}{False\ Positive} \tag{10}$$

IV. RESULTS AND DISCUSSION

A. PRE-PROCESSING RESULTS

20GB datasets containing set of infinite MTC nuclei were pre-processed [Figure4] to [Figure 8] and threshold segmentation was applied to reduce the noise. Eccentric nuclei were processed with the seed analysis algorithms and mean of regional maxima based round circles were plotted. Random edge demographic quantities were recorded in dataset. Since the distance matrix was used to measure the abnormal behaviors of circles around the nuclei for training and testing of

TABLE 2. Nuclei centre and nucleus point plotting.

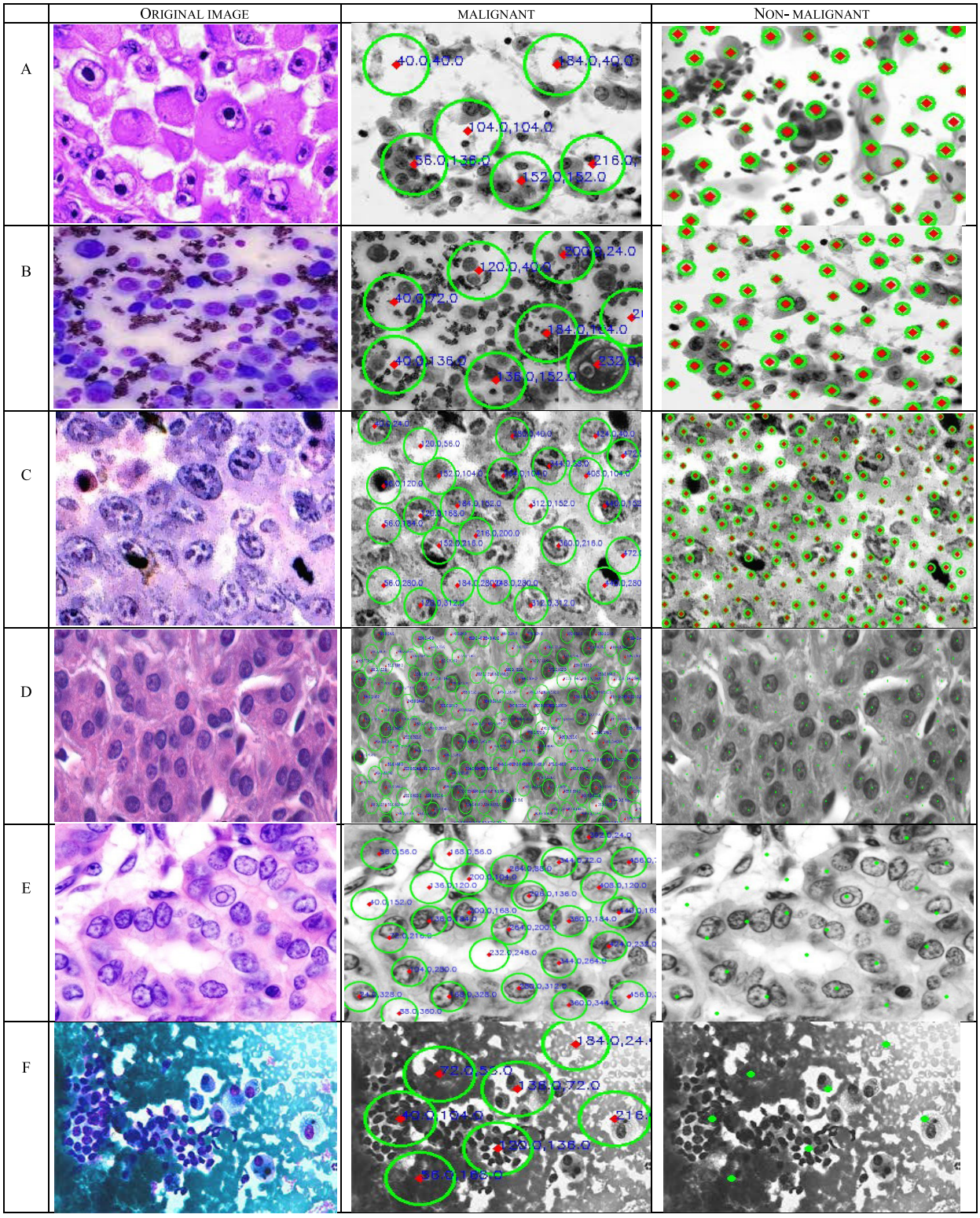

CNN classifier. Group of eccentric nuclei were encircled as region of interest and nuclei separation process was applied to auto-crop the sub images so called nuclei. Each nuclei was separated from each other and the properties of the nuclei were recorded. Each nuclei's chromatin levels were measured and colour movements were also recorded in separate dataset

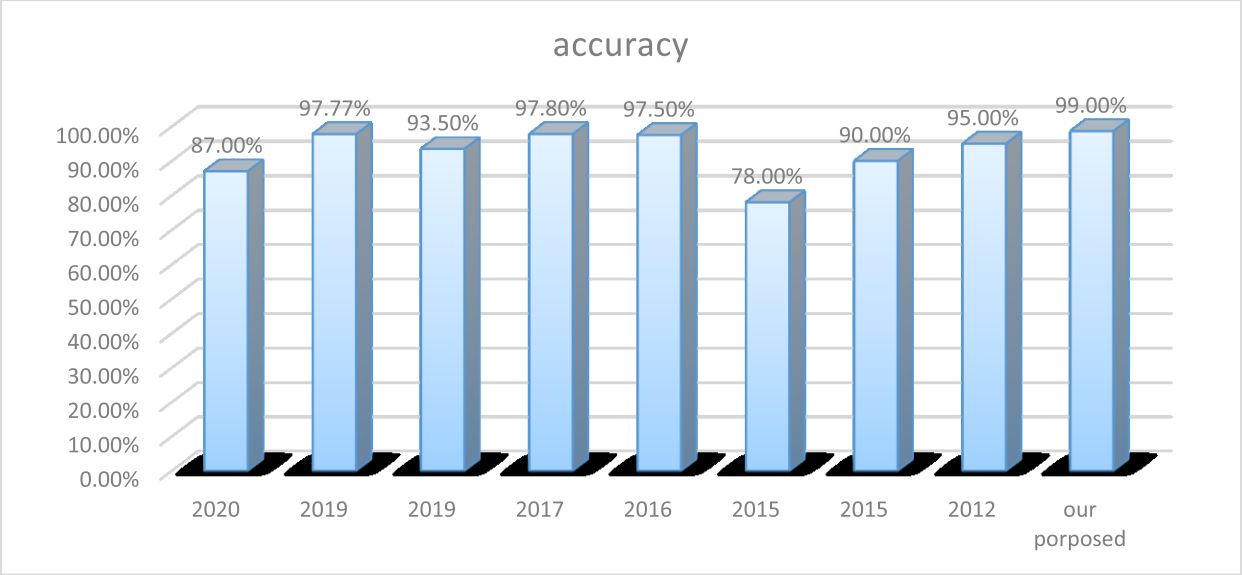

FIGURE 10. Comparison of our approach with literature.

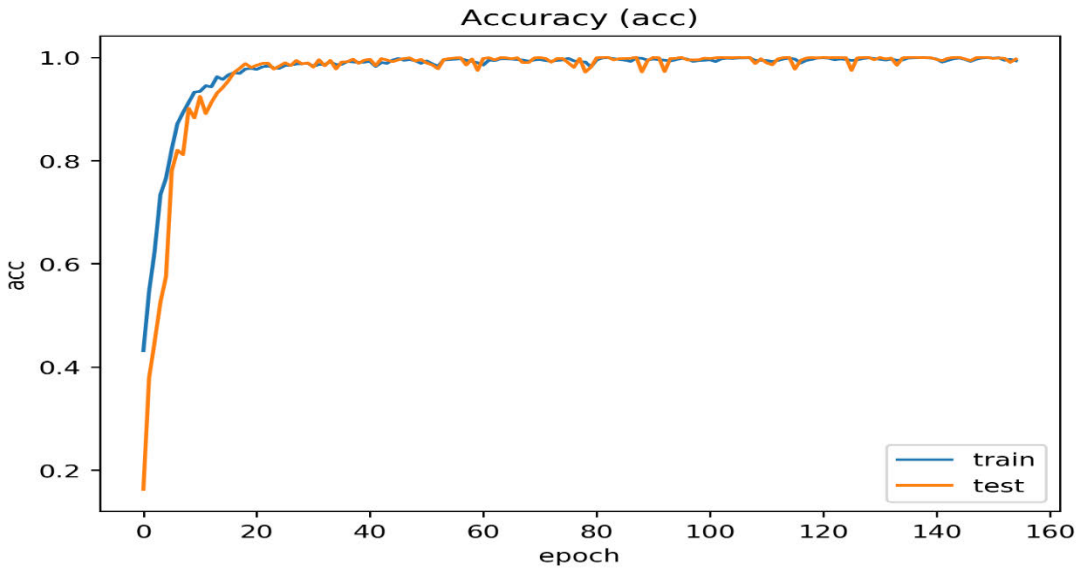

FIGURE 11. Train and test curves.

TABLE 3. Confusion matrix.

	MALIGNANT	NON- MALIGNANT
Malignant	3521	29
Non- Malignant	27	2024

as future work. Tensor T datasets were recorded to train and test the nuclei sets by using convolutional neural network.

B. CLASSIFICATION RESULTS

This article addresses the classification problem of Medullary Thyroid Cancer and classifies malignant and non-malignant cells and tissues. The system selects pixel level micro architectural components of every nuclei. The proposed methodology of this article is comprising upon three layers. Layer one is designated as image processing and where segmentation, find coordinate, find intersections, approx. size of nuclei are extracted and each individual nuclei is cropped. Since the changes in nucleus is very essential to detect at initial stage. Overall classification accuracy of the system is measured as 99.00 percent and confusion matrix [Table 3] visualizes that there are 5601 observations classified as malignant class label attribute and 2053 observations were considered as non- malignant class by the classifier. Precision for malignant class is measured as 99.18 percent and recall approximation is recorded as 98.68 per-

TABLE 4. Overall performance of proposed methodology.

	Raw DICOM images	No of Extracted nuclei	No of classified Nuclei	No of miss-classified Nuclei	Precession	Over all accuracy
Malignant	60	2860	3521	29	99.18%	99.32%
Non-Malignant	40	575	2024	27	98.68%	98.58%

TABLE 5. Thyroid cancer classification accuracy comparison as per literature.

Year	Approaches	Image Type 1- Ultrasound, 2- FNAC, 3 – FNAB	Thyroid Cancer (1-Follicular, 2-Papillary, 3-Anaplast, 4-Medullary)	Classification Accuracy
2020	01	3	1	87.00%
2019	02	3	1-2-3-4	100%, 100%, 98.89, 97.77%
2019	03	1	2	93.50%
2017	04	3	2	97.8%
2016	1	1	1	97.50 %
2015	3	1	1	78.00%
2015	4	2	1	90.00%
2012	5	2	1	95.00%
Our Proposed approach		3	4	99.00%

TABLE 6. Summary of experiment based on CNNs.

Epoch	Time in seconds	loss	Accuracy %
1/5 (3548 x 3548)	7	0.1361	95.91
2/5 (3548 x 3548)	5	0.0416	98.74
3/5 (3548 x 3548)	5	0.0298	99.09
4/5 (3548 x 3548)	5	0.0219	99.28
5/5 (3548 x 3548)	5	0.0177	99.44
Total Loss	0.0356	Commutative Accuracy	99.00

cent [Table 4]. Precision for non- malignant class label attribute is recorded as 98.68 percent and recall estimated as 98.58 percent. [Table 5] presents comparison of this approach with other approaches existing in literature. Graphical chart [Figure 9] shows that our proposed literature has highest accuracy with comparison to literature. In [Table 2] several cytological images are shown from A to E, where original image, malignant and non-malignant columns are visualized. In image [A] original image reveals that three are six places where malignant cells or nuclei are detected and encircled with diameter which is calculated from the distance matrix, meanwhile non- malignant class plotted in nearby column. Likewise image (B), (C), (D), (E) are showing original image, malignant regions and non – malignant nuclei. In [Table 6] overall accuracy and total loss is calculated against each epoch. Epoch one consumed 07 seconds and 0.1361 loss was recorded whereas 95.91% accuracy was estimated. Epoch two consumed 05 seconds and 0.0416 loss was estimated whereas 98.74% accuracy was estimated. Epoch three took 05 seconds to process and produced 0.0298 loss meanwhile accuracy 99.09% was recorded. Epoch four 05 seconds with loss estimated as 0.0219 and accuracy was measured as 99.28%. Epoch five processed 05 seconds and generated

0.0177 loss, whereas 99.44% accuracy was estimated. Total loss was measured 0.0356 and 99.00% overall accuracy was recorded. Training and testing plot has been shown in [Figure 10]. Histopathology is one the reliable method to diagnose the types of cancer which is very vital for prognosis. The system separated 5601 nuclei by using the methods as presented in methodology section. CNNs are reliable to construct the decision model there tensor T datasets were created for training and testing purposes at middle layer and the lower level layer was assigned to evaluate the performance evaluation were confusion matrix, precision and recall measure was used. Malignant and non – malignant nuclei are visualized in [Table 2]. Overall classification accuracy of the system 99.00 percent whereas 3521 observations were classified as malignant and 2024 observation were classified as non- malignant for MTC. Total loss was measured 0.0356 and 99.00% overall accuracy was recorded. Training and testing plot has been shown in [Figure 10]. This article contributes that (i) each nuclei has given equal chance to be classified (ii) eccentric nuclei properties are visualized (iii) highest classification accuracy 99.00% for MTC has been proposed whereas previous proposed accuracy 97.77%.

ACKNOWLEDGMENT

The authors would like to say special thanks to SMBBMU, Pakistan, for providing datasets.

REFERENCES

[1] J. Begum and R. Samal, "A clinicopathological evaluation of post-menopausal bleeding and its correlation with risk factors for developing endometrial hyperplasia and cancer: A hospital-based prospective study," *J. Mid-life Health*, vol. 10, no. 4, p. 179, 2019.

[2] E. Ozdemir and C. Gunduz-Demir, "A hybrid classification model for digital pathology using structural and statistical pattern recognition," *IEEE Trans. Med. Imag.*, vol. 32, no. 2, pp. 474–483, Feb. 2013.

[3] M. Salvi, U. Morbiducci, F. Amadeo, R. Santoro, F. Angelini, I. Chimenti, D. Massai, E. Messina, A. Giacomello, M. Pesce, and F. Molinari, "Automated segmentation of fluorescence microscopy images for 3D cell detection in human-derived cardiospheres," *Sci. Rep.*, vol. 9, no. 1, pp. 1–11, Dec. 2019.

[4] O. Faust, Y. Hagiwara, T. J. Hong, O. S. Lih, and U. R. Acharya, "Deep learning for healthcare applications based on physiological signals: A review," *Comput. Methods Programs Biomed.*, vol. 161, pp. 1–13, Jul. 2018.

[5] J. Angel Arul Jothi and V. Mary Anita Rajam, "A survey on automated cancer diagnosis from histopathology images," *Artif. Intell. Rev.*, vol. 48, no. 1, pp. 31–81, Jun. 2017.

[6] Y. S. Vang and Z. C. X. Xie, "Deep learning framework for multi-class breast cancer histology image classification," in *Proc. Int. Conf. Image Anal. Recognit.* Cham, Switzerland: Springer, 2018.

[7] D. Ardila, A. P. Kiraly, S. Bharadwaj, B. Choi, J. J. Reicher, L. Peng, D. Tse, M. Etemadi, W. Ye, G. Corrado, D. P. Naidich, and S. Shetty, "End-to-end lung cancer screening with three-dimensional deep learning on low-dose chest computed tomography," *Nature Med.*, vol. 25, no. 6, pp. 954–961, Jun. 2019.

[8] M. J. Cha, M. J. Chung, J. H. Lee, and K. S. Lee, "Performance of deep learning model in detecting operable lung cancer with chest radiographs," *J. Thoracic Imag.*, vol. 34, no. 2, pp. 86–91, Mar. 2019.

[9] T. Iwasawa, K. Okudela, T. Takemura, T. Fukuda, S. Matsushita, T. Baba, T. Ogura, M. Tajiri, and A. Yoshizawa, "Computer-aided quantification of pulmonary fibrosis in patients with lung cancer: Relationship to disease-free survival," *Radiology*, vol. 292, no. 2, pp. 489–498, Aug. 2019.

[10] A. Das, U. R. Acharya, S. S. Panda, and S. Sabut, "Deep learning based liver cancer detection using watershed transform and Gaussian mixture model techniques," *Cognit. Syst. Res.*, vol. 54, pp. 165–175, May 2019.

[11] A. Brunetti, L. Carnimeo, G. F. Trotta, and V. Bevilacqua, "Computer-assisted frameworks for classification of liver, breast and blood neoplasias via neural networks: A survey based on medical images," *Neurocomputing*, vol. 335, pp. 274–298, Mar. 2019.

[12] V. Sharma and K. C. Juglan, "Ultrasound-based classification of fatty liver disease: A review," in *Proc. J. Phys., Conf.*, vol. 1531, no. 1. Bristol, U.K.: IOP Publishing, 2020, Art. no. 012033.

[13] Z. Zhang, P. Chen, M. McGough, F. Xing, C. Wang, M. Bui, Y. Xie, M. Sapkota, L. Cui, J. Dhillon, N. Ahmad, F. K. Khalil, S. I. Dickinson, X. Shi, F. Liu, H. Su, J. Cai, and L. Yang, "Pathologist-level interpretable whole-slide cancer diagnosis with deep learning," *Nature Mach. Intell.*, vol. 1, no. 5, pp. 236–245, May 2019.

[14] E. Y. Jeong, H. L. Kim, E. J. Ha, S. Y. Park, Y. J. Cho, and M. Han, "Computer-aided diagnosis system for thyroid nodules on ultrasonography: Diagnostic performance and reproducibility based on the experience level of operators," *Eur. Radiol.*, vol. 29, no. 4, pp. 1978–1985, Apr. 2019.

[15] J. H. Lee, E. J. Ha, and J. H. Kim, "Application of deep learning to the diagnosis of cervical lymph node metastasis from thyroid cancer with CT," *Eur. Radiol.*, vol. 29, no. 10, pp. 5452–5457, Oct. 2019.

[16] D. A. Omondiagbe, S. Veeramani, and A. S. Sidhu, "Machine learning classification techniques for breast cancer diagnosis," in *Proc. IOP Conf., Mater. Sci. Eng.*, vol. 495, no. 1. Bristol, U.K.: IOP Publishing, 2019, Art. no. 012033.

[17] M. N. Reza, I. S. Na, S. W. Baek, and K.-H. Lee, "Rice yield estimation based on K-means clustering with graph-cut segmentation using low-altitude UAV images," *Biosyst. Eng.*, vol. 177, pp. 109–121, Jan. 2019.

[18] H. Yu, F. He, and Y. Pan, "A novel segmentation model for medical images with intensity inhomogeneity based on adaptive perturbation," *Multimedia Tools Appl.*, vol. 78, no. 9, pp. 11779–11798, May 2019.

[19] J. Dogra, S. Jain, and M. Sood, "Analysis of graph cut technique for medical image segmentation," in *Proc. Int. Conf. Adv. Inform. Comput. Res.* Singapore: Springer, 2019, pp. 451–463.

[20] H. Li, W. L. Thorstad, K. J. Biehl, R. Laforest, and Y. Su, "A novel PET tumor delineation method based on adaptive region-growing and dual-front active contours," *Med. Phys.*, vol. 35, no. 8, pp. 3711–3721, 2008.

[21] L. Zhang, G. Zeng, and J. Wei, "Adaptive region-segmentation multi-focus image fusion based on differential evolution," *Int. J. Pattern Recognit. Artif. Intell.*, vol. 33, no. 03, Mar. 2019, Art. no. 1954010.

[22] T. A. Tuan, J. Y. Kim, and P. T. Bao, "Adaptive region growing for skull, brain, and scalp segmentation from 3D MRI," *Biomed. Eng., Appl., Basis Commun.*, vol. 31, no. 05, Oct. 2019, Art. no. 1950033.

[23] J. Schlemper, O. Oktay, M. Schaap, M. Heinrich, B. Kainz, B. Glocker, and D. Rueckert, "Attention gated networks: Learning to leverage salient regions in medical images," *Med. Image Anal.*, vol. 53, pp. 197–207, Apr. 2019.

[24] K.-J. Xia, H.-S. Yin, and J.-Q. Wang, "A novel improved deep convolutional neural network model for medical image fusion," *Cluster Comput.*, vol. 22, no. S1, pp. 1515–1527, Jan. 2019.

[25] A. Fourcade and R. H. Khonsari, "Deep learning in medical image analysis: A third eye for doctors," *J. Stomatol., Oral Maxillofacial Surg.*, vol. 120, no. 4, pp. 279–288, Sep. 2019.

[26] Z. Marinković, G. Crupi, and A. Caddemi, "A review on the artificial neural network applications for small-signal modeling of microwave FETs," *Int. J. Numer. Model., Electron. Netw., Devices Fields*, vol. 33, no. 3, p. e2668, 2020.

[27] E. Chaves, C. B. Gonçalves, M. K. Albertini, S. Lee, G. Jeon, and H. C. Fernandes, "Evaluation of transfer learning of pre-trained CNNs applied to breast cancer detection on infrared images," *Appl. Opt.*, vol. 59, no. 17, p. E23, Jun. 2020.

[28] R. Kasmi and K. Mokrani, "Classification of malignant melanoma and benign skin lesions: Implementation of automatic ABCD rule," *IET Image Process.*, vol. 10, no. 6, pp. 448–455, 2016.

[29] D. Dov, S. Ziv Kovalsky, S. Assaad, A. A. Pendse Jonathan Cohen, D. Elliott Range, R. Henao, and L. Carin, "Weakly supervised instance learning for thyroid malignancy prediction from whole slide cytopathology images," 2019, *arXiv:1904.12739*. [Online]. Available: http://arxiv.org/abs/1904.12739

[30] Y. Wang, Q. Guan, I. Lao, L. Wang, Y. Wu, D. Li, Q. Ji, Y. Wang, Y. Zhu, H. Lu, and J. Xiang, "Using deep convolutional neural networks for multi-classification of thyroid tumor by histopathology: A large-scale pilot study," *Ann. Transl. Med.*, vol. 7, no. 18, p. 468, Sep. 2019.

[31] H. Li, J. Weng, Y. Shi, W. Gu, Y. Mao, Y. Wang, and W. Liu, "An improved deep learning approach for detection of thyroid papillary cancer in ultrasound images," *Sci. Rep.*, vol. 8, p. 6600, Apr. 2018.

[32] G. A. Ashamallah and M. A. EL-Adalany, "Risk for malignancy of thyroid nodules: Comparative study between TIRADS and US based classification system," *Egyptian J. Radiol. Nucl. Med.*, vol. 47, no. 4, pp. 1373–1384, Dec. 2016.
[33] D. W. Kim, J. S. Park, H. S. In, and H. J. Choo, "Ultrasound-based diagnostic classification for solid and partially cystic thyroid nodules," *Amer. J. Neuroradiol.*, vol. 33, no. 6, pp. 1144–1149, 2012.
[34] S.-Y. Tay, C.-Y. Chen, and W. P. Chan, "Sonographic criteria predictive of benign thyroid nodules useful in avoiding unnecessary ultrasound-guided fine needle aspiration," *J. Formosan Med. Assoc.*, vol. 114, no. 7, pp. 590–597, Jul. 2015.
[35] A. S. Negm, O. A. Hassan, and A. H. Kandil, "A decision support system for acute leukaemia classification based on digital microscopic images," *Alexandria Eng. J.*, vol. 57, no. 4, pp. 2319–2332, Dec. 2018.
[36] P. Viswanathan, "Fuzzy c means detection of leukemia based on morphological contour segmentation," *Procedia Comput. Sci.*, vol. 58, pp. 84–90, 2015.
[37] H. A. N. Zulfanahri, E. L. Frannita, I. Ardiyanto, and L. Choridah, "Computer aided diagnosis for thyroid cancer system based on internal and external characteristics," *J. King Saud Univ.-Comput. Inf. Sci.*, to be published.
[38] Y. J. Yoo, E. J. Ha, Y. J. Cho, and H. L. Kim, "Computer-aided diagnosis of thyroid nodules via ultrasonography: Initial clinical experience," *Korean J. Radiol.*, vol. 19, no. 4, pp. 665–672, 2018.

JAMIL AHMED CHANDIO was born in Larkana, Sindh, Pakistan. He received the bachelor's and M.S./M.Phil. degrees in computer science from Shah Abdul Latif University, Khairpur, in 2004 and 2009, respectively.

Since 2000, he has been working at the IT Department, Larkana Institute of Nuclear Medicine and Radiotherapy (LINAR), Pakistan. He has been working as a Visiting Faculty Member at Sukkur IBA University and the SZABIST Larkana, Pakistan, since 2014. He supervised ten final year projects (research-based) at graduate levels. He is the author of about several number of research articles, published in international repute journals and research papers published in the proceedings of national and international conferences. His research interests include medical image mining, artificial intelligence, digital image processing, and deep learning.

GHULAM ALI MALLAH received the master's degree from Quaid-i-Azam University Islamabad and the Ph.D. degree in computer science on HEC sponsorship and the Postdoctorate degree in educational technology from Glasgow University, Scotland, U.K., on sponsorship of the British Council. He is currently the Head of computer science with Shah Abdul Latif University, Khairpur, Pakistan. His research interests include software agents, artificial intelligence, digital image processing, and so on. He has visited more than a dozen countries to present his research work. He has more than 40 HEC recognized national and international research articles at his credit. He has supervised two dozen M.S./Ph.D. students. He is actively involved in various national and international professional bodies for quality assurance in HEIs, curriculum designing, accreditations, tertiary education support program, development of strategic and business plans for HEIs, and international linkages. He is a member of various national and international academic forums/bodies, including the IEEE and ACM. He is the Winner of 04 HEC-Funded Research and Development Projects and the ICT Excellence Award in the category of IT Education. He is the Organizer of the four consecutive International Conferences on Computer and Emerging Technologies and one International Conference on Research in Education and Technologies, in 2017.

NOOR AHMED SHAIKH was born in Khairpur, Sindh, Pakistan, in 1967. He received the degree in computer systems engineering from the Mehran University of Engineering and Technology, Jamshoro, Pakistan, in 1989, and the Ph.D. degree in computer science from Shah Abdul Latif University, Khairpur, in 2009.

From 1990 to 1994, he worked as a System Analyst and the System Analyst cum Lecturer and an Assistant Professor, from 1994 to 2011. Since 2011, he has been working as a Professor at the Department of Computer Science, Shah Abdul Latif University. He supervised two Ph.D. and two M.S./M.Phil. graduates and supervising three Ph.D. and four M.S./M.Phil. students. He is the author of about three dozens of research articles, published in international repute journals and a dozen of research papers published in the proceedings of national and international conferences. His research interests include digital image processing, natural language processing, and deep learning. He was a recipient of the HEC Indigenous Ph.D. Scholarship. He is the Editor-in-Chief of the *International Journal of Computer Science and Emerging Technologies*. He has organized four international conferences and an editor of their proceedings.